



# Present-Day Crustal Deformation Within the Western Qinling Mountains and Its Kinematic Implications

Ming Hao<sup>1,2</sup> · Yuhang Li<sup>1</sup> · Qingliang Wang<sup>1</sup> · Wenquan Zhuang<sup>1</sup> · Wei Qu<sup>3</sup>

Received: 26 May 2020 / Accepted: 21 October 2020 / Published online: 24 November 2020  
© Springer Nature B.V. 2020

## Abstract

The western Qinling Mountains, located between the East Kunlun fault and the West Qinling fault, hold the key to investigating the outward expansion of the Tibetan Plateau. We use up-to-date GPS observations to derive high spatial–temporal resolution crustal velocity and strain rate fields for this region. Our results suggest that a series of NEE-trending faults bounding the eastern margin of the western Qinling Mountains experience right-lateral strike slip with low rates of ~1 mm/yr. In addition, our results suggest that crustal deformation of the western Qinling Mountains could be governed by a right-lateral shear zone trending NNE at a rate of ~6 mm/yr, producing a clockwise rotation of subblocks: left-lateral and right-lateral strike slip on the NWW-trending and NEE-trending faults, respectively. The eastward extrusion of the Tibetan Plateau along the western Qinling Mountains is limited further east. In contrast, the NNE-ward expansion of the northeastern Tibetan Plateau is the primary motion which extends through the western Qinling Mountains and the Longxi block. The results of this study improve our understanding of the outward expansion of the Tibetan Plateau influenced by the Indian–Eurasian collision.

**Keywords** Western Qinling Mountains · Eastward expansion · Crustal movement · Block model · Right-lateral shear zone

---

**Electronic supplementary material** The online version of this article (<https://doi.org/10.1007/s10712-020-09621-5>) contains supplementary material, which is available to authorized users.

---

✉ Ming Hao  
ha\_mg@163.com

<sup>1</sup> The Second Monitoring and Application Center, China Earthquake Administration, Xi'an 710054, China

<sup>2</sup> Southern Laboratory of Ocean Science and Engineering Guangdong Laboratory, Zhuhai 519082, China

<sup>3</sup> College of Geology Engineering and Geomatics, Chang'an University, Xi'an 710054, China

## 1 Article Highlights

1. High spatial–temporal resolution of crustal velocity and strain fields for western Qinling Mountains.
2. Crustal deformation of western Qinling Mountains could be governed by a right-lateral shear zone trending NNE.
3. NNE-ward expansion of Tibetan Plateau is the primary motion, while eastward extrusion is limited.

## 2 Introduction

The northeastern Tibetan Plateau is a transition zone connecting the Tibetan Plateau and the North China–Pacific plate, and it is also the junction of tectonic structures striking EW and NS in mainland China (Tapponnier et al. 1982; Zhang et al. 1995, 2004; Mercier et al. 2013). Large-scale left-lateral strike-slip fault systems trending EW, such as the East Kunlun fault and the Haiyuan fault, indicate significant eastward extrusion of the Tibetan plateau. At the same time, development of several right-lateral strike-slip faulting structures trending NNE, such as the northern segment of the Longmenshan fault zone, the Longriba fault, and the Yinchuan graben, suggests northward movement of the plateau (Deng et al. 1999; Xu et al. 2008, 2017; Shi et al. 2020). Although the two groups of structures above can be attributed to the context of northeastward expansion of the Tibetan Plateau, whether their tectonic deformation is dominated by the eastward extrusion or northward expansion of the plateau and how the two groups of deformation interact in a unified kinematics scheme remain in dispute.

Numerous kinematic models have been proposed to delineate different deformation processes of the northeastern Tibetan Plateau, based on large fault offsets and left-lateral strike-slip rates on the East Kunlun fault and the Haiyuan fault inferred from geological (Van der Woerd et al. 2002; Li et al. 2005, 2009; Kirby et al. 2007, 2013) and GPS-derived crustal deformation (Zuza and Yin 2016; Li et al. 2018). One model stresses the significance and importance of the eastward lateral extrusion of the crustal material in the plateau (Peltzer et al. 1985; Tapponnier et al. 2001; Jiang et al. 2003; Zhang et al. 1995; Ma et al. 2013). Considering geological records of clear left-lateral strike slip along the eastern Qinling Mountains, either the East Kunlun–Qinling Mountains fault system (Jiang et al. 2003; Zhang et al. 1995; Ma et al. 2013) or the Haiyuan–Liupanshan–Qinling Mountains fault system (Peltzer et al. 1985; Tapponnier et al. 2001) is regarded as the channel for the eastward escape of the plateau and the connection for influencing the tectonic deformation of the North China Plain in the late Quaternary. Constraining from geological and geodetic measurements, another model suggests that the eastward extrusion of the northeastern Tibetan Plateau along the East Kunlun fault and the Haiyuan fault is resisted by the rigid block-like motion of the South China and the Ordos block (Kirby et al. 2007; Harkins and Kirby 2008; Kirby and Harkins 2013; Zheng et al. 2016; Zuza and Yin 2016; Li et al. 2018). Moreover, the deformation is accommodated by thrusting on the eastern tip of the faults, crustal shortening, and mountain uplift in the western Qinling Mountains. Hence, the eastward extrusion is largely confined within the plateau (Kirby et al. 2007; Harkins and Kirby 2008; Kirby and Harkins 2013; Zheng et al. 2016; Li et al. 2018). England and

Molnar (1990) indicated that there is significant northward movement in the northeastern Tibetan Plateau, and a prominent right-lateral shear deformation zone trending NNE is formed between the plateau and the stable Sichuan basin (Kirby and Harkins 2013). According to this second model, the right-lateral shear deformation controls left-lateral strike slip on the EW-trending faults of the northern Tibetan Plateau in the pattern of the bookshelf fault model (Zuza and Yin 2016).

These models suggest different crustal deformation patterns and slip rates on the major active faults within the northeastern Tibetan Plateau, especially the EW-trending East Kunlun and West Qinling faults, and a series of secondary active fault systems consisting of the NWW-trending and NEE-trending between them. It is challenging to record geological slip rates on faults with small offsets in the western Qinling Mountains, where the multiple NWW-trending, NEE-trending and arcuate faults intersect (Duvall and Clark 2010). Geodetic observation can be used to probe deformation of millimeter-scale accuracy and is well suited for monitoring regional crustal movement and slip rates on faults. Previous studies have provided various GPS velocity fields for the western Qinling Mountains (Ge et al. 2013; Liang et al. 2013; Zheng et al. 2017; Wang and Shen 2020). These GPS results suggest that the East Kunlun fault and the Haiyuan fault experience prominent left-lateral strike-slip deformation, and the slip rates decrease eastward and transfer to crustal contraction and folding (Zheng et al. 2013; Li et al. 2018). In addition, geological and geodetic data imply that the deformation of the Haiyuan fault and Alxa block is influenced by significant northward movement of the northeastern Tibetan Plateau (Duvall and Clark 2010). These studies expand our understanding of tectonic deformation of the northeastern Tibetan Plateau, but it is hard to quantify present characteristics of faults between the West Qinling and East Kunlun faults, and reveal the regional deformation patterns more completely.

In this study, a GPS horizontal velocity field spanning from 1999 to 2019 with high spatiotemporal resolution was acquired by additional observations from our recent field geodetic works. Then, the slip rate on faults of the west Qinling Mountains was estimated by using GPS velocities. A deformable block motion model was employed to characterize the movements of nine tectonic terranes in this region. Our study provides new constraints on deciphering the outward expansion of the Tibetan Plateau: The NNE-ward expansion of the northeastern Tibetan Plateau is the primary motion which extends through the western Qinling Mountains. However, the eastward extrusion of the Tibetan Plateau along the western Qinling Mountains is limited further east.

### 3 Regional Tectonic Setting

The western Qinling Mountains are located between the East Kunlun fault and the West Qinling fault and are recognized as the step-over of these two major left-lateral strike-slip faults (Yuan et al. 2004). Previous studies suggest that the left-lateral strike-slip rates along the East Kunlun fault decrease from  $> 10$  to  $< 2$  mm/yr toward its eastern tip (Van der Woerd et al. 2002; Guo et al. 2007; Kirby et al. 2007; Lin and Guo 2008; Duvall and Clark 2010; Li et al. 2011; Diao et al. 2019), while the West Qinling fault has low left-lateral slip rates of 2–3 mm/yr (Li et al. 2007; Shao et al. 2011; Ge et al. 2013; Li et al. 2015).

Within the western Qinling Mountains, two sets of active faults trending NWW and NEE are located at its western and eastern parts, respectively. The former mainly consists of the Lintan-Tanchang fault, the Guanggaishan-Dieshan fault, the Bailongjiang fault, and

the Tazang fault. The latter includes the Lixian-Luojiabao fault, the Chengxian-Taibai fault, and the Wenxian-Kangxian fault (Fig. 1).

Recent geological studies have documented the constraints of slip rate on these faults. The Lintan-Tanchang fault is a left-lateral strike-slip and thrust fault, which hosted the 2013  $M_s$  6.6 Minxian earthquake (Zheng et al. 2013). The estimated strike-slip rate has been  $\sim 1$  mm/yr since the late Quaternary (Liu 2012). The Guanggaishan-Dieshan fault experiences left-lateral strike slip with thrusting deformation (Yu et al. 2012). The field investigations, satellite image analysis, and structural data reveal that the left-lateral strike-slip rate of the late Quaternary on the Bailongjiang fault is 1.7–2.6 mm/yr (Li et al. 2019). Moreover, the Tazang fault, the easternmost segment of the East Kunlun fault, has left-lateral strike-slip rates of 1.3–3.2 and 0.2–0.3 mm/yr on its west and east sections, respectively (Ren et al. 2013). The 2017  $M_s$  7.0 Jiuzhaigou earthquake occurred on the Huya fault connecting the Tazang fault to the south (Xu et al. 2017; Sun et al. 2018).

With respect to the east section of the western Qinling Mountains, previous studies suggested that the Lixian-Luojiabao fault is a left-lateral strike-slip fault with a slip rate of 0.95 mm/yr since the late Quaternary (Han et al. 2001). Additionally, the 1654  $M$  8 southern Tianshui earthquake occurred on this fault (Yang et al. 2015). The Chengxian-Taibai fault bounding the Chengxian basin on the north has left-lateral strike-slip and thrust dip-slip rates of  $0.71 \pm 0.18$  and  $0.43 \pm 0.13$  mm/yr (Zheng et al. 2016), respectively. Other studies have revealed that the Lixian-Luojiabao fault and the Chengxian-Taibai fault experience right-lateral shear deformation instead of left-lateral deformation, which responds to

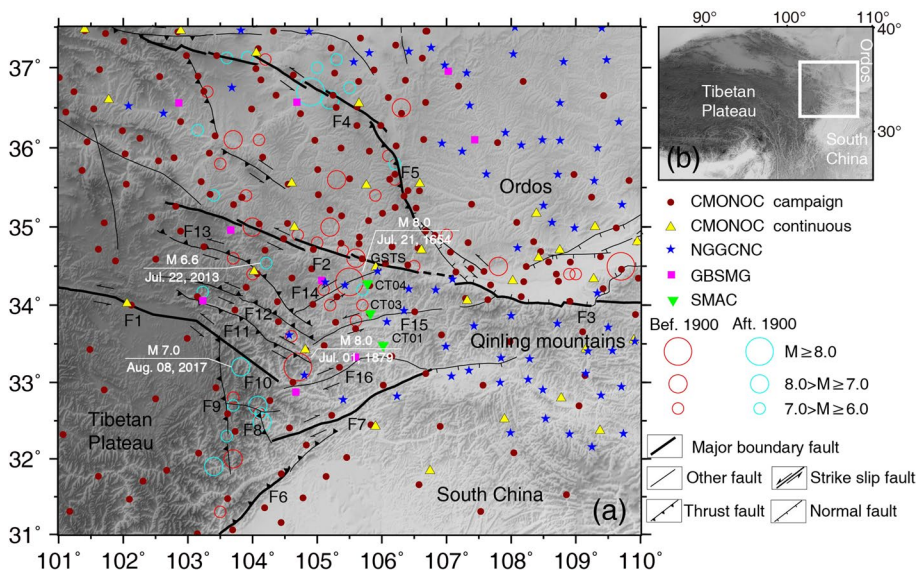


**Fig. 1** Tectonic setting of the western Qinling Mountains, showing active faults, earthquakes, and GPS stations. The white rectangle in (b) shows our study area. Earthquakes represented as circles (a) are from China Earthquake Data Center (<http://data.earthquake.cn>). Abbreviations used are: East Kunlun fault (F1), West Qinling fault (F2), Qinling Piedmont fault (F3), Haiyuan fault (F4), Liupanshan fault (F5), Longmenshan fault zone (F6), Pingwu-Qingchuan fault (F7), Huya fault (F8), Mingjiang fault (F9), Tazang fault (F10), Bailongjiang fault (F11), Guanggaishan-Dieshan fault (F12), Lintan-Tanchang fault (F13), Lixian-Luojiabao fault (F14), Chengxian-Taibai fault (F15), and Wenxian-Kangxian fault (F16)

the northward expansion of the Tibetan Plateau (Xu et al. 2017; Shi et al. 2020). Although the Wenxian-Kangxian fault is determined to be a left-lateral strike-slip fault bounding the north margin of the stable Bikou block, its slip rate remains ambiguous (Wang et al. 2001; Jia et al. 2012). Which seismogenic fault produced the 1879  $M$  8 southern Wudu earthquake is still controversial (Hou et al. 2005; Yuan et al. 2014; Li et al. 2019) due to the absence of well-preserved surface ruptures, but there is consensus that the epicenter of this earthquake was located at the intersection of the Bailongjiang fault and the Wenxian-Kangxian fault (Fig. 1). To summarize, the broad distribution of active faults, together with frequent strong earthquakes, implies the region of study is undergoing complex tectonic deformation.

## 4 Data and Methods

GPS data used in our study were mainly obtained from the key national scientific infrastructure project of the Crustal Movement Observation Network of China (CMONOC). The campaign GPS stations were resurveyed every 2 or 3 years from 1999 to 2019, and the continuous GPS stations in the western Qinling Mountains have been operational since 2010. Additionally, we collected data from campaign GPS stations from the National GPS Geodetic Control Network of China (NGGCNC), which conducted the first survey in 2005 or 2014; surveys were conducted again twice by the Second Monitoring and Application Center (SMAC) and the China Earthquake Administration in 2012 and 2018–2019, respectively. We also collected GPS data from Continuous Operation Reference Stations (CORS) recorded in 2014–2018 by the Gansu Bureau of Surveying Mapping and Geoinformation (GBSMG). In order to monitor activity of the Chengxian-Tianbai fault, the SMAC has installed three continuous GPS stations across this fault since October 2017. Figure 1 shows that GPS stations from the NGGCNC and GBSMG are a necessary supplement in space for the CMONOC in the western Qinling Mountains.

The GAMIT package (Herring et al. 2015a) was utilized to process the double differenced carrier-phase data to obtain loosely constrained daily solutions for satellite orbits, station coordinates, tropospheric zenith delays, and their variances–covariances matrix. The IONEX files (provided by the Center for Orbit Determination in Europe) containing total electron content (TEC) at 2-h intervals were adopted to mitigate high-order ionospheric delays. We also process GPS data of ~ 70 International Terrestrial Reference Frame (ITRF) core stations with the same model to get global loosely constrained daily solutions. Then, the regional daily solutions were combined with global solutions and then fixed to ITRF2014 (Altamimi et al. 2017) by utilizing the GLOBK package (Herring et al. 2015b). In the last step, we calculated the GPS station position time series.

The GPS position time series in our study area were affected by two large earthquakes: the 2008  $M_S$  8.0 Wenchuan, China earthquake, and the 2011  $M_S$  9.0 Tohoku-Oki, Japan earthquake. To reduce the coseismic offsets of the Wenchuan earthquake from the campaign station time series, the Kriging method was employed to interpolate the coseismic displacement field given by Shen et al. (2009). Then, the interpolated coseismic offsets were used to correct the time series. For the effect of postseismic displacements following this earthquake, we only used GPS data measured before 2008 for stations within the post-seismic deformation region determined by Wang and Shen (2020). Hao and Zhuang (2020) provided the coseismic displacement field of the 2011 Tohoku-Oki earthquake using more GPS stations located in the eastern China and found that this event affected the region east

of  $105^{\circ}\text{E}$ , and the postseismic deformation was confined in the northeastern China and eastern portions of North China. Therefore, we also used the Kriging method to interpolate coseismic displacements to correct the campaign GPS time series and neglect the postseismic deformation. Finally, we employed the weighted least squares method to fit position time series and derive the linear velocity with respect to ITRF2014.

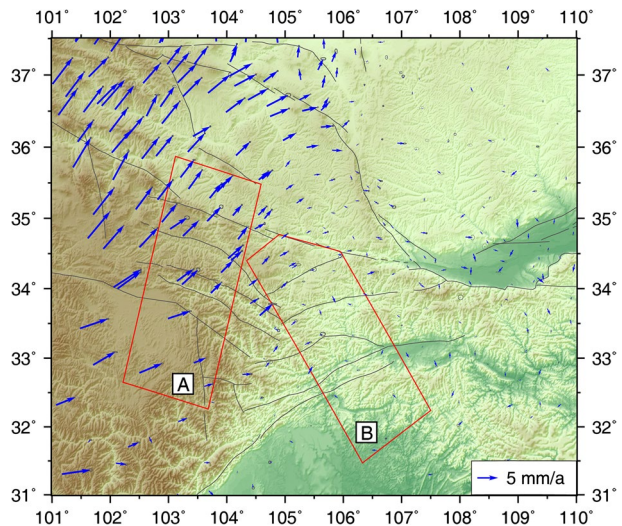
In order to represent differential horizontal movements within the western Qinling Mountains, we selected its adjacent stable Ordos block as a regional reference frame. We chose the GPS velocities located on the Ordos block to estimate the Euler pole with the assumption of the block boundaries freely slipping. We employed the weighted least squares by applying constraints that minimized motions within the interior of the Ordos block. We ruled out potential outliers from the velocities through an iterative procedure: The stations with the largest post-fit residual were removed and re-calculated the angular velocity until all the post-fit residuals were less than 2 mm/yr. With respect to ITRF2014, we estimated the Ordos block Euler pole of  $75.083^{\circ}\text{N} \pm 0.850^{\circ}$  and  $139.692^{\circ}\text{W} \pm 3.701^{\circ}$ , with an angular rotation rate of  $0.352 \pm 0.006^{\circ}/\text{Ma}$ . Finally, we transformed the velocities into the Ordos-fixed frame (Fig. 2). The GPS velocity field is provided in supplementary material.

## 5 Results

### 5.1 Strain Rate Field

As shown in Fig. 2, the crustal velocities are divided into two parts by about  $105^{\circ}\text{E}$ , where the west section moves NNE-ward and the east section deforms insignificantly. To visualize the crustal deformation of the studied region, we calculate the strain rate field by using the method of a continuous function developed by Shen et al. (2015). This method interpolates a set of discrete GPS velocities and introduces the spatial weighting function with smoothing distance  $D$  optimally determined according to the in situ data quality. It is robust because it does not depend on certain assumptions on data. As shown in Fig. 3a, the

**Fig. 2** GPS velocity field with respect to the Ordos-fixed frame. Red polygons show locations of the GPS velocity profiles in Fig. 6. The orientation of profiles *A* and *B* is  $\text{N}13^{\circ}\text{E}$  and  $\text{N}30^{\circ}\text{W}$ , respectively. Error ellipses denote  $1 - \sigma$  uncertainties



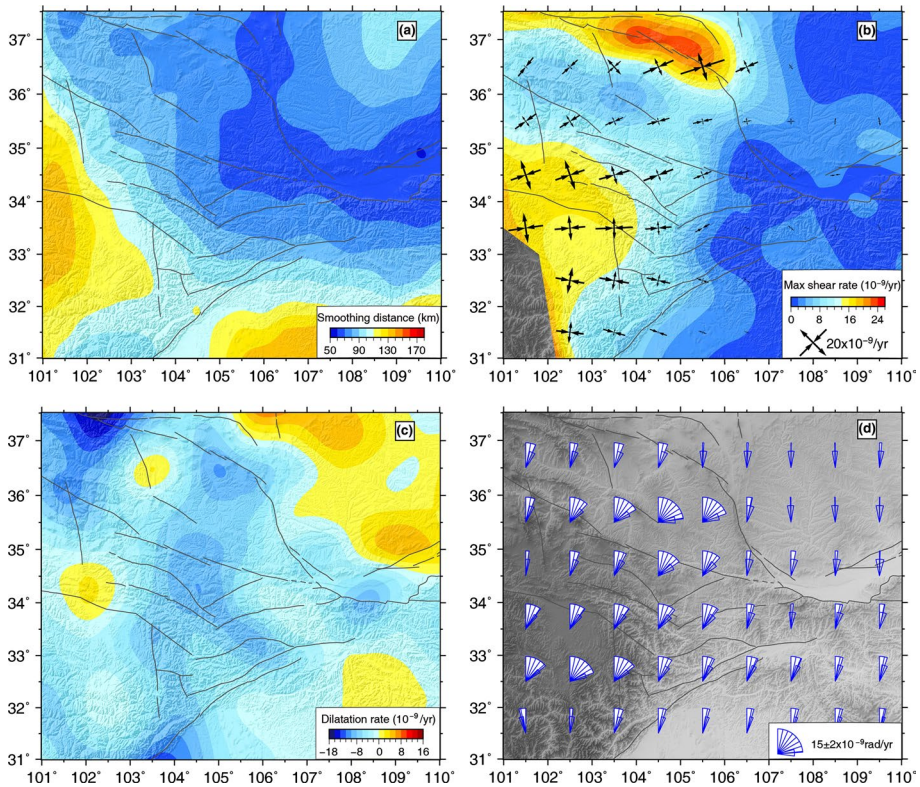


**Fig. 3** Strain rate fields for the western Qinling Mountains. **a** Spatial smoothing distance used in GPS velocity interpolation. **b** The maximum shear strain and principal strain rates. **c** Dilatation rate (areal contraction negative). **d** Rotation rate (clockwise rotation positive)

smallest  $D$  of about 50 km is along the southeastern margin of the Ordos block, where the GPS stations are the most densely distributed. Across the western Qinling Mountains, the smoothing distances are 60–80 km due to our updated dense GPS data.

The maximum shear strain rate in Fig. 3b shows that significant shear strain rates of  $16\text{--}24 \times 10^{-9}/\text{yr}$  appear in the Haiyuan fault and the East Kunlun fault, where the primary strain rates are the largest too. Our estimated maximum shear strain rate across the Haiyuan fault is much lower than the result in Li et al. (2018), but consistent with Zheng et al. (2017) and Wang and Shen (2020). The orientation of compressive strain changes from nearly EW around the Kunlun fault to NE around the Haiyuan fault. The primary strain and the maximum shear strain rates in the east of  $105^\circ\text{E}$  are insignificant, which is similar to the results of Wang and Shen (2020). The dilatation rate in Fig. 3c indicates that the western Qinling Mountains and the surroundings are mainly in contractional deformation. There is a N–S trending contraction zone along about  $105^\circ\text{E}$ , where the strain rates calculated by Li et al. (2018) and Wang and Shen (2020) also appear approximately. On the intersection region between the NWW-trending and NEE-trending faults, the areal contraction rate is up to  $12 \times 10^{-9}/\text{yr}$ . Figure 3d demonstrates that the region between the East Kunlun fault and the Haiyuan-Liupanshan fault behaves in a clockwise rotation, and the rotation rate is increasing and then decreasing gradually to the eastward, where the largest

clockwise rotation rate of up to  $15 \times 10^{-9}$  rad/yr is found at the center of the Longxi block located between the West Qinling fault and the Haiyuan-Liupanshan fault (Wang and Shen 2020). The rotation rate across the Longxi block is larger than that across its west and east regions. On the south of the East Kunlun fault, the rotation rate reduces from west to east, demonstrating the decreasing shear deformation toward the eastern tip of the East Kunlun fault. The rotation rate is little across the Ordos block.

## 5.2 GPS Velocity Profiles and Baseline Length Changes

We construct two GPS velocity profiles across the NWW-trending and NEE-trending faults, which are shown in Fig. 2. Profile A passes through the Tazang, Guanggaishan-Dieshan, Lintan-Tanchang, and West Qinling faults. The N13°E components (parallel to the profile) (Fig. 4a) suggest  $\sim 1$  mm/yr crustal shortening across regions between the Tazang and West Qinling faults, but little shortening across each of them. The N103°E components (normal to the profile) (Fig. 4b) imply  $\sim 3$  mm/yr left-lateral shear across the region between the Tazang and West Qinling faults. Specifically, the Tazang, Guanggaishan-Dieshan, and West Qinling faults experience left-lateral shear deformation of  $1.6 \pm 0.1$ ,  $0.9 \pm 0.2$  and  $0.4 \pm 0.3$  mm/yr, respectively. The Lintan-Tanchang fault has no obvious strike-slip deformation.

Profile B strikes N30°W across the Pingwu-Qingchuan, Wenxian-Kangxian, Chengxian-Taibai, and Lixian-Luojiabao faults. Figure 4c also shows undetectable shortening across the region between the Pingwu-Qingchuan and West Qinling faults, and the velocity components normal to the profile (Fig. 4d) indicate right-lateral shear of  $\sim 2.5$  mm/yr within this region. The right-lateral slip rates of  $0.8 \pm 0.2$ ,  $0.7 \pm 0.2$  and  $1.8 \pm 0.2$  mm/yr are

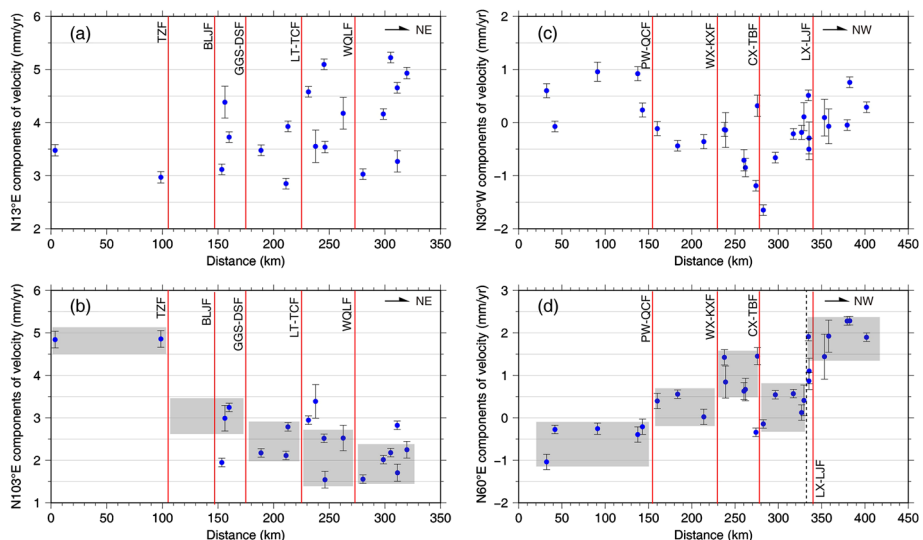


**Fig. 4** GPS velocity profiles across the western Qinling Mountains. **a–d** show the GPS velocity components parallel and normal to direction of profiles *A* and *B*. Dashed line in **(d)** shows a velocity gradient zone. Abbreviations are Tazang fault (TZF), Bailongjiang fault (BLJF), Guanggaishan-Dieshan fault (GGS-DSF), Lintan-Tanchang fault (LT-TCF), West Qinling fault (WQLF), Pingwu-Qingchuan fault (PW-QCF), Wenxian-Kangxian fault (WX-KXF), Chengxian-Taibai fault (CX-TBF), and Lixian-Luojiabao fault (LX-LJF)



on the Pingwu-Qingchuan, Wenxian-Kangxian, and Lixian-Luojiabao faults, respectively. There is a left-lateral slip rate of  $0.8 \pm 0.2$  mm/yr on the Chengxian-Taibai fault. Particularly, our GPS profile reveals a velocity gradient zone (here named “Nianguangba deformation zone”) located about 10 km south of and parallel to the Lixian-Luojiabao fault. In fact, the right-lateral slip rate of 1.8 mm/yr across the Lixian-Luojiabao fault is mainly accommodated by its south velocity gradient, which demonstrates complex tectonic activity in the western Qinling Mountains.

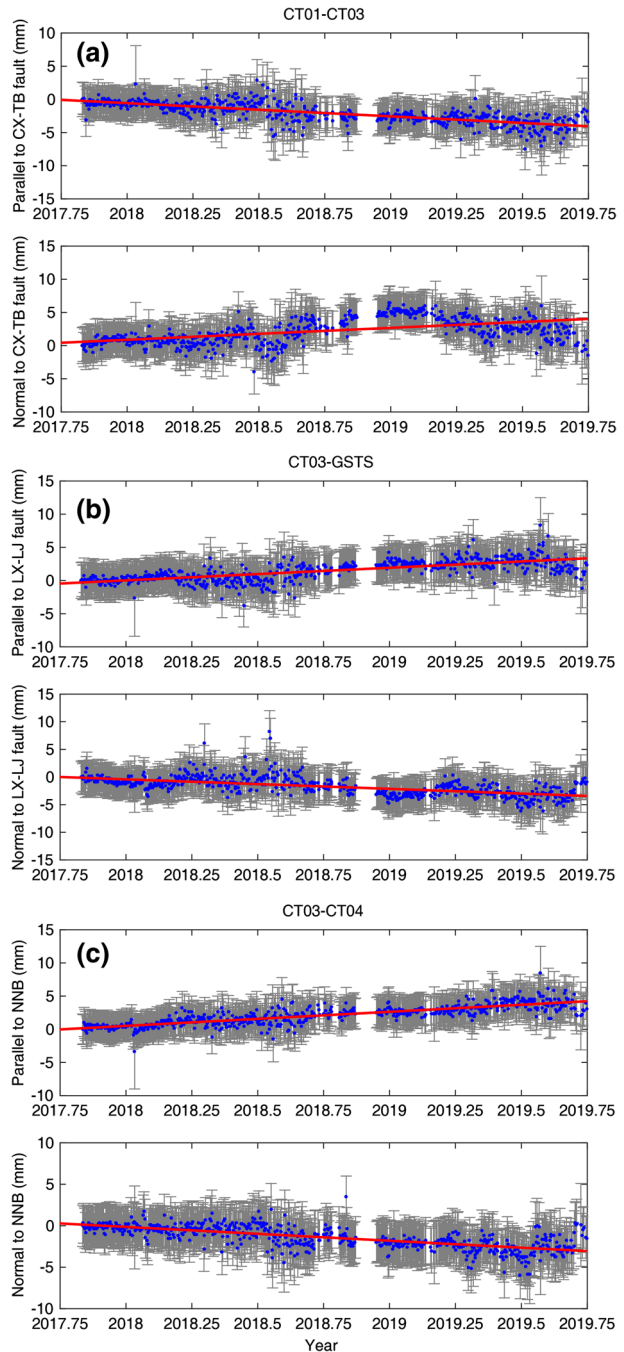
Additionally, three continuous GPS stations (CT01, CT03, and CT04 in Fig. 1) across the Chengxian-Taibai fault have been operational since October 2017. Therefore, we calculate the baseline length change across this fault and the Lixian-Luojiabao fault using GPS data of these three stations and one continuous station (GSTS) from the CMONOC. We decomposed the baseline change into two components: parallel and normal to the fault. As shown in Fig. 5a, the baseline CT01–CT03 across the Chengxian-Taibai fault and the parallel and normal components suggested a right-lateral slip rate of  $2.0 \pm 0.1$  and extensional slip rate of  $1.8 \pm 0.1$  mm/yr on this fault. The parallel and normal components of length changes for baseline CT03–GSTS across the Lixian-Luojiabao fault (Fig. 5b) show that this fault deforms  $2.1 \pm 0.1$  mm/yr right-lateral shear and  $1.7 \pm 0.1$  mm/yr shortening. The baseline CT03–CT04 passes through the Nianguangba deformation zone, and the parallel and normal components (Fig. 5c) show  $1.9 \pm 0.1$  mm/yr right-lateral and  $1.7 \pm 0.1$  mm/yr shortening deformation across this gradient zone. The baseline changes imply that the deformation across the Lixian-Luojiabao fault is not obvious, but the velocity gradient zone to its south demonstrates significant right-lateral shear, which is consistent with the GPS velocity profile.

### 5.3 Block Motion

We employed the deformable block motion model (Shen et al. 2015) in order to reveal characteristics of crustal deformation in the western Qinling Mountains respective to its adjacent tectonic terranes. Using the model, we estimated the block translation and rotation parameters with respect to the Ordos block and the internal uniform strain rates of the block without considering locking on the block boundary. Zhang et al. (2003) proposed that active tectonic blocks are geological units that have been separated from each other by active tectonic zones, which represent significant gradient of differential movement. And most of tectonic activities occur on the blocks’ boundaries. In addition, the boundaries of tectonic blocks may follow those of old geological units, but may also be newly formed during the latest tectonic deformation in the late Cenozoic (Zhang et al. 2003). Based on this assumption, the blocks are bounded by the primary and secondary active faults within the western Qinling Mountains. We defined nine blocks around the western Qinling Mountains based on the distribution of GPS stations and previous block division results (Zhang et al. 2003; Ge et al. 2013; Rui and Stamps 2016; Zheng et al. 2016; Li et al. 2018, 2019): Longxi (LX), Minxian (MX), Bailongjiang (BL), Bayan Har (BH), Bikou (BK), Chengxian (CX), Xihe (XH), South China (SC), and Ordos (OR) blocks. The block motion model results are shown in Fig. 6 and listed in Table 1.

With respect to the Ordos block, the block motion model results suggest that the Bayan Har, Bailongjiang, Minxian, and Longxi blocks on the west move from the inner Tibetan Plateau toward outside along the NE direction, the velocity rates decrease from 5.7 to 2.8 mm/yr gradually, and these blocks undergo compressive strain deformation directing EW or NEE. The South China block on the east moves SW-ward at a rate of 2.1 mm/yr. The Xihe,

**Fig. 5** Baseline length changes across faults. **a**, **b**, and **c** show components of baseline changes parallel and normal to the Chengxian-Taibai fault (CX-TB) striking  $N80^{\circ}E$ , the Lixian-Luojiabao fault (LX-LJ) and the Niangniangba deformation zone (NNB) striking  $N70^{\circ}E$ , respectively. Red lines denote the fitting linear rates for the components of baseline changes



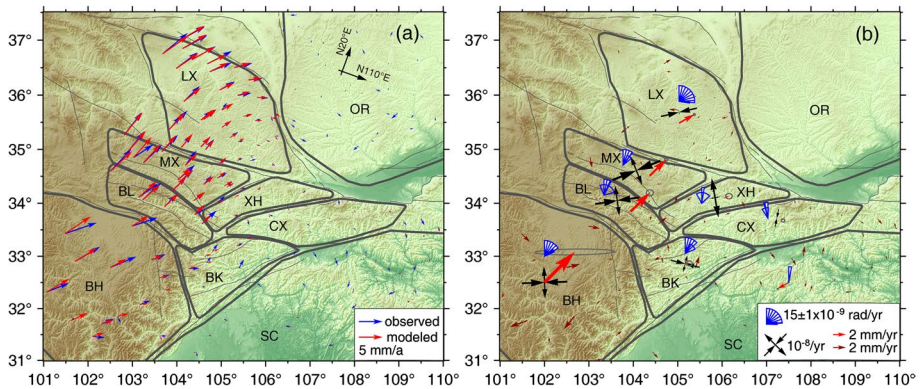


**Fig. 6** Block motion model around the western Qinling Mountains. **a** Observed GPS velocities (blue vectors) and predicted (red vectors). **b** Block translation (red vectors), rotation (blue fan shape), internal uniform strain rates (black crossing arrows), and post-fit residuals (dark red vectors). Thick and thin gray lines are block boundaries and active faults

Chengxian, and Bikou blocks between them demonstrate negligible translation movement and ambiguous internal strain owing to large uncertainty (Table 1). The Longxi, Bayan Har, Minxian, Bailongjiang, and Bikou blocks move in a clockwise rotation, and the Longxi block has the largest rate of  $16.6 \times 10^{-9}$  rad/yr, while the Chengxian and Xihe blocks in the east of the western Qinling Mountains do not show clear rotation.

To further delineate differential deformation behavior of tectonic blocks, the GPS velocities in the Longxi, Minxian, and Bailongjiang blocks are projected to the directions of N20°E and N110°E, normal and parallel to the strike direction of the West Qinling fault (Figs. 6a and Fig. 7). The result from the N20°E components of velocity illustrates that from the west of the western Qinling Mountains to the east of the Longxi block, northward movement is significant. This could be recognized as the main channel for strain transformation of the Tibetan Plateau (Duvall and Clark 2010). Furthermore, this northward strain transformation is decreasing eastward along the West Qinling fault (Fig. 7a), which is consistent with a lower strain rate distribution (Fig. 3). The decreasing northward movement from west to east results in a large right-lateral shearing deformation with a rate of  $\sim 6$  mm/yr, which could be the regional kinematics governing the right-lateral strike-slip faults trending NEE, including the Lixian-Luojiabao, Chengxian-Taibai, and Pingwu-Qingchuan faults (Figs. 4 and 5). The right-lateral shear trending NNE over the northeastern Tibetan Plateau accounts for clockwise rotation of subblocks (Fig. 6b).

The N110°E components of velocity (Fig. 7b) from south to north suggest that right-lateral shear deformation of  $\sim 3$  mm/yr trending EW bounds the Longxi block, which produces the eastward extrusion and clockwise rotation of the Longxi block. Together with right-lateral shear trending NNE, clockwise rotation of the Longxi block is larger than that of the western Qinling Mountains. Comparing to eastward movement of 2–4 mm/yr in the Longxi block, the eastward extrusion of the western Qinling Mountains is much lower ( $\sim 2$  mm/yr), indicating that shear strain transferring to its eastern part is even less.

**Table 1** Results of deformable block motion model

Block	Reference point		Translation <sup>a</sup>		Rotation <sup>b</sup> (10 <sup>-9</sup> rad/yr)	Internal strain rate		Direction <sup>c</sup> (°)	τ <sub>e</sub> (10 <sup>-9</sup> /yr)	τ <sub>en</sub> (10 <sup>-9</sup> /yr)	τ <sub>n</sub> (10 <sup>-9</sup> /yr)
	Lon. (°E)	Lat. (°N)	E (mm/yr)	N (mm/yr)		Ext. (10 <sup>-9</sup> /yr)	Com. (10 <sup>-9</sup> /yr)				
LX	105.029	35.685	2.4±0.1	1.4±0.1	16.6±0.8	1.5±1.5	-11.7±1.6	257.0±3.2	-11.1±1.1	-2.9±0.7	0.8±1.0
MX	104.069	34.607	2.6±0.1	2.6±0.1	6.4±2.5	9.8±5.5	-16.3±3.5	248.1±5.4	-12.7±2.3	-9.1±2.4	6.2±4.3
BL	103.639	34.046	3.1±0.3	2.9±0.2	4.7±8.6	9.6±21.6	-14.1±13.4	261.9±20.6	-13.6±7.8	-3.3±8.6	9.2±14.5
XH	105.842	34.098	0.8±0.2	0.2±0.2	1.6±6.9	12.7±18.9	-3.2±7.6	260.0±24.7	-2.7±3.1	-2.7±6.9	12.2±13.0
CX	107.232	33.719	0.3±0.1	-0.4±0.1	-2.7±3.1	0.8±3.2	-5.8±7.8	191.6±26.4	0.5±1.4	-1.3±3.1	-5.6±5.4
BK	105.170	32.856	0.7±0.2	0.1±0.2	8.3±3.5	5.4±8.0	-9.4±5.0	103.9±13.3	-8.6±3.0	3.5±3.5	4.6±5.6
BH	101.350	32.725	4.9±0.2	2.9±0.2	10.3±1.3	10.2±2.6	-14.4±2.6	268.0±2.9	-14.4±1.6	-0.9±1.3	10.2±1.6
SC	111.636	27.233	-1.8±0.1	-1.0±0.1	1.8±0.1	0.7±0.1	-0.5±0.1	123.4±2.3	-0.2±0.06	0.5±0.05	0.3±0.07

<sup>a</sup>East and northward movement positive

<sup>b</sup>Clockwise rotation positive

<sup>c</sup>Direction of the compressive strain rate clockwise from north

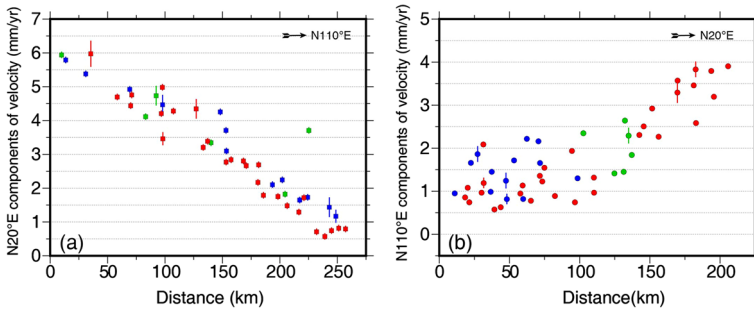


**Fig. 7** **a** GPS velocity of N20°E components from west to east. **b** GPS velocity of N110°E components from south to north. The red, blue, and green dots represent the GPS velocities within the Longxi, Minxian, and Bailongjiang blocks, respectively. The GPS velocities within each block are shown in Fig. 6a

## 6 Discussion

### 6.1 Fault Slip Rate

Based on our dense GPS results, the slip rates on major active faults of the western Qinling Mountains are estimated from GPS profiles and baseline length changes (Figs. 4 and 5). Table 2 lists the slip rates derived from our GPS data and previous geological measurements. The Tazang fault has a left-lateral slip rate of  $1.6 \pm 0.1$  mm/yr, similar to the late Quaternary slip rate of 1.3–3.2 mm/yr inferred from geomorphic surface offsets and dating (Ren et al. 2013). The Guanggaishan-Dieshan fault has a left-lateral slip rate of 0.9 mm/yr, close to 0.51 mm/yr of geological slip rate in the late Quaternary (Yu et al. 2012). There are no detectable left-lateral strike-slip signals across the Bailongjiang fault and the Lintan-Tanchang fault from our GPS profile (Fig. 4b). The West Qinling fault has a left-lateral slip rate of 0.4 mm/yr, much lower than the geological constraint of 2–3 mm/yr in the late Quaternary (Li et al. 2007). But our estimated low slip rate on the West Qinling fault is consistent with the GPS result given by Ge et al. (2013). As a matter of fact, excluding the

**Table 2** Comparison of slip rates (in mm/yr) derived from GPS and geological measurements

Fault name	GPS-derived slip rate (this study)	Geology-derived slip rate
Tazang	$1.6 \pm 0.1$ L	1.3–3.2 L (Ren et al. 2013)
Bailongjiang	–	1.7–2.6 L (Li et al. 2019)
Guanggaishan-Dieshan	$0.9 \pm 0.2$ L	$0.51 \pm 0.13$ L (Yu et al. 2012)
Lintan-Tanchang	Insignificant	1 L (Liu 2012; Zheng et al. 2016)
West Qinling	$0.4 \pm 0.3$ L	2–3 L (Li et al. 2007)
Lixian-Luojiaobao	Insignificant	0.95 L (Han et al. 2001)
Niangniangba	$1.8 \pm 0.2$ R	–
Chengxian-Taibai	$0.8 \pm 0.2$ L	$0.71 \pm 0.18$ L (Zheng et al. 2016)
Wenxian-Kangxian	$0.7 \pm 0.2$ R	–
Pingwu-Qingchuan	$0.8 \pm 0.2$ R	0.7 R (Sun 2015)

L and R mean left-lateral and right-lateral strike slip, respectively

1718 M<sub>7.5</sub> Tongwei earthquake which occurred on the middle segment of the West Qinling fault, there has been no large earthquake occurred on the eastern and western segment. Probably, the western segment our GPS velocity crossed is locking, and the seismic risk should be paid more attention.

As we can see, the left-lateral slip rate across the NWW-trending faults on the west section of the western Qinling Mountains is only 3–4 mm/yr (Fig. 4b), which is much lower than a total left-lateral slip rate of 6.5–10.3 mm/yr according to the late Quaternary geological estimations, including slip rates of 1.3–3.2 mm/yr on the Tazang fault (Ren et al. 2013), 1.7–2.6 mm/yr on the Bailongjiang fault (Li et al. 2019), 0.51 mm/yr on the Guanggaishan-Dieshan fault (Yu et al. 2012), 1 mm/yr on the Lintan-Tanchang fault (Liu et al. 2012; Zheng et al. 2016), and 2–3 mm/yr on the West Qinling fault (Li et al. 2007). Both the uncertainty of geological measurement and the possibility of fault slip rate varying with time could result in this discrepancy. Moreover, right-lateral shear deformation trending NNE could also produce permanent displacements on the NWW-trending faults through earthquake occurrence, which can be recorded by the geological method. Because the GPS data reveal the interseismic crustal deformation, we cannot fully see that part of the deformation due to the influence of elastic locking on faults (Zhang et al. 2018). So, it is reasonable to explain the discrepancy on left-lateral strike-slip rate between geological and geodetic studies. Our results imply that NNE-ward movement of the northeastern Tibetan Plateau plays a key role in the regional crustal deformation.

For the faults that are NEE trending on the east section of the western Qinling Mountains, our results show that these faults experience right-lateral strike-slip deformation (Fig. 4d). The determined right-lateral slip rate of 0.8 mm/yr on the Pingwu-Qingchuan fault is close to the geological slip rate of 0.7 mm/yr since the late Quaternary (Sun 2015). The GPS-derived left-lateral slip rate of 0.8 mm/yr on the Chengxian-Taibai fault is consistent with study of Zheng et al. (2016). However, the GPS baseline length changes suggest that the Chengxian-Taibai fault demonstrates right-lateral and extensional faulting activities. The inconsistency probably arises because the strike-slip deformation on the Chengxian-Taibai fault is slight and the baseline changes across the fault have only been observed for less than 2 years (Fig. 5). Although geological studies show that the Lixian-Luojiabao fault is a left-lateral strike-slip fault with slip rate of less than 1 mm/yr (Han et al. 2001), our results reveal that shear deformation across the Lixian-Luojiabao fault is insignificant, while a velocity gradient zone on its south has a right-lateral strike-slip rate of ~2 mm/yr. The NNE-trending right-lateral shear over the northeastern Tibetan Plateau plays a crucial part in right-lateral strike slip on NEE-trending faults at the east section of the western Qinling Mountains.

## 6.2 Crustal Deformation Pattern

The characteristics of crustal movement and fault slip rate provide primary constraints for understanding the deformation pattern. Zheng et al. (2016) employed the bookshelf model to describe the motion of subblocks in the western Qinling Mountains. It was emphasized that the clockwise rotation of subblocks controls left-lateral strike slip on faults trending NWW and NEE. However, the kinematic model for clockwise rotation is not well established, and it is hard to explain right-lateral strike slip on the NEE-trending faults, which is determined by recent geological studies (Xu et al. 2017; Shi et al. 2020) and our GPS measurements. In contrast, Shi et al. (2020) stressed that large-scale right-lateral shear roughly trending NNE could dominate deformation around the Ordos block, but this hypothesis has

not been tested by present-day crustal deformation constraints, and was not employed to study the western Qinling Mountains in this study.

Here, based on previous studies and derived GPS measurements of this work, we propose a bookshelf model governed by the right-lateral shear zone with NNE direction to delineate regional crustal deformation and faulting activities (Fig. 8b). It shows that the western Qinling Mountains lies in the velocity gradient of ~6 mm/yr trending NNE, which drives clockwise rotation of subblocks, and left- and right-lateral strike slip on the NWW- and NEE-trending faults, respectively (Fig. 8a). Additionally, the left-lateral strike-slip faults trending NWW also experience thrusting deformation (Zheng et al. 2016; Li et al. 2019; Zhang et al. 2018) to accommodate horizontal compressive strain (Fig. 3b).

The proposed kinematic model delineates the crustal horizontal movement, where the driving force originates from northeastward expansion of the Tibet Plateau (Fig. 8a). The leveling-derived vertical velocity (Hao et al. 2016) suggests that the northeastern Tibet uplifts at different rates, and Tianshui (northeast corner of the Minxian block) uplifts at maximum rate of 6 mm/yr. The budget of horizontal material influx implies that excessive material influx into the lower crust or upper mantle underneath most region seems required to maintain the large uplift rates. Teleseismic receiver functions reveal that Tianshui and its neighboring regions with high  $V_p$  and  $V_p/V_s$  values close to uplifts of magma and hot springs might result from the upwelling of mantle materials induced by the expansion. To provide a three-dimensional kinematic model, more works are needed in a future study.

### 6.3 Outward Growth of the Northeastern Tibetan Plateau

The western Qinling Mountains connect the Tibetan Plateau to the west and the Qinling Mountains to the east. Therefore, the crustal deformation and faulting activity are the key to answering the controversial discussion of the eastward extrusion of the Tibetan Plateau.

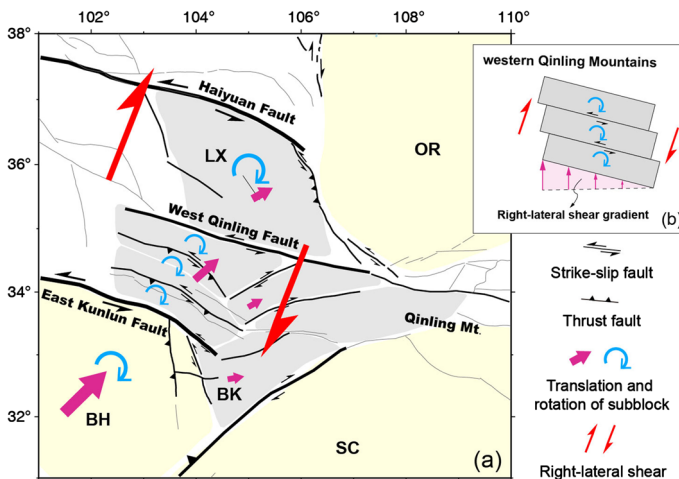


**Fig. 8** **a** Present-day crustal deformation pattern of the western Qinling Mountains and its adjacent areas (gray shadow represents the main area of the western Qinling Mountains). **b** Conceptual diagram showing the pattern of faulting and crustal deformation controlled by right-lateral shear without considering inner and boundary deformation

Previous studies show that the left-lateral strike-slip rate on the East Kunlun fault decreases eastward from  $> 10$  mm/yr on the central part to  $< 2$  mm/yr on the eastern segment of Tazang fault and the eastern terminal of East Kunlun fault (Van der Woerd et al. 2002; Kirby et al. 2007; Li et al. 2011; Ren et al. 2013; Li et al. 2019). So, the eastward extrusion along the East Kunlun fault is restrained within the Tibetan Plateau and transformed to crustal shorting, thrusting, and uplifting (Kirby et al. 2007; Li et al. 2018). The slight left-lateral strike-slip rate of  $\sim 1$  mm/yr on each fault trending NWW implies that the eastward extrusion along the western Qinling Mountains is also limited and originates from the right-lateral shear gradient trending NNE. Moreover, the derived right-lateral strike-slip rates on a series of faults trending NEE further illustrate that the eastward extrusion could have little influence on deformation of the Qinling Mountains (Fig. 8a).

Our results support the theory that there is NNE-ward movement of the northeastern Tibetan Plateau across the western Qinling Mountains to the Yinchuan graben further north (Shi et al. 2020). The prominent right-lateral shear in the direction of NNE going through the western Qinling Mountains and the Longxi block (Fig. 8a) indicates that the northeastern Tibetan Plateau represents northward movement primarily instead of the eastward extrusion. The eastern boundary of northward movement is outlined by the N–S trending contraction zone along  $105^\circ\text{E}$ , where its west moves NNE-ward and its east deforms insignificantly (Fig. 8).

## 7 Conclusions

We derived an up-to-date GPS horizontal tectonic velocity field with high spatial–temporal resolution for the western Qinling Mountains and analyzed the characteristics of strain distribution and fault slip rates on active faults. Major conclusions of this study include the following:

1. A series of NEE-trending faults bounding the eastern margin of the western Qinling Mountains experience right-lateral strike slip with lower rates of  $\sim 1$  mm/yr, constrained by GPS data. Among these faults, a velocity gradient zone to the south of and parallel to the Lixian-Luojiabao fault has a relative high right-lateral slip rate of  $1.8 \pm 0.2$  mm/yr.
2. The crustal deformation pattern of the western Qinling Mountains could be governed by a large right-lateral shear zone trending NNE with rate of  $\sim 6$  mm/yr. We suggest this is the main reason for clockwise rotation of subblocks, left- and right-lateral strike slip on the NWW- and NEE-trending faults between the East Kunlun fault and the West Qinling fault, respectively.
3. The eastward extrusion of the Tibetan Plateau along the western Qinling Mountains is limited further east. By contrast, the NNE-ward expansion of the northeastern Tibetan Plateau is the primary motion which passes through the western Qinling Mountains and the Longxi block.

**Acknowledgements** We thank the National Administration of Surveying, Mapping and Geoinformation and the Gansu Bureau of Surveying Mapping and Geoinformation for sharing a part of the GPS data used in this study. We also thank all the crew of the CMONOC project for their hard work. We sincerely thank two anonymous reviewers and the Associate Editor Prof. Jeff Gu for their constructive comments and suggestions. This work was supported by grants from the National Key Research and Development Program



of China (2017YFC1500102), the National Natural Science Foundation of China (41874017, 41874117), the Science for Earthquake Resilience (XH19067Y), the Second Tibetan Plateau Scientific Expedition and Research Program (2019QZKK0901), and the Guangdong Province Introduced Innovative R&D Team of Geological Processes and Natural Disasters around the South China Sea (2016ZT06N331). The GPS velocity solution is provided as supplementary material and archived at the Harvard Dataverse Web site (<https://doi.org/10.7910/DVN/5X9OXQ>), separately.

## Compliance with Ethical Standards

**Conflict of interest** The authors declare that they have no conflict of interest.

## References

- Altamimi Z, Métivier L, Rebischung P, Rouby H, Collilieux X (2017) ITRF2014 plate motion model. *Geophys J Int* 209:1906–1912
- Deng QD, Cheng SP, Min W, Yang GZ, Ren DW (1999) Tectonic activity and dynamic of the Ordos block. *J Geomech* 5(3):13–21 (**in Chinese**)
- Diao F, Xiong X, Wang R, Walter TR, Wang Y, Wang K (2019) Slip rate variation along the Kunlun fault (Tibet): results from new GPS observations and a viscoelastic earthquake-cycle deformation model. *Geophys Res Lett* 46(5):2524–2533
- Duvall AR, Clark MK (2010) Dissipation of fast strike-slip faulting within and beyond northeastern Tibet. *Geology* 38:223–226
- England P, Molnar P (1990) Right-lateral shear and rotation as the explanation for strike-slip faulting in eastern Tibet. *Nature* 344(6262):140–142
- Ge WP, Wang M, Shen ZK, Yuan DY, Zheng WJ (2013) Interseismic kinematics and deformation patterns on the upper crust of Qaidam-Qilianshan block. *Chin J Geophys* 56(9):2994–3101 (**in Chinese**)
- Guo J, Lin A, Sun G, Zheng J (2007) Surface ruptures associated with the 1937 M 7.5 Tuosuo Lake and the 1963 M 7.0 Alake Lake earthquakes and the paleoseismicity along the Tuosuo Lake segment of the Kunlun fault, northern Tibet. *Bull Seismol Soc Am* 97(2):474–496
- Han ZJ, Xiang HF, Ran YK (2001) Active analysis of Lixian-Luojiapu fault zone in the east boundary of Tibetan Plateau since the late-Pleistocene. *Seismol Geol* 23(1):43–48 (**in Chinese**)
- Hao M, Zhuang WQ (2020) The impact of the great 2011 Tohoku-Oki earthquake on crustal deformation in eastern China. *J Geodesy Geodyn* 40(6):138–142 (**in Chinese**)
- Hao M, Wang Q, Cui D, Liu L, Zhou L (2016) Present-day crustal vertical motion around the Ordos block constrained by precise leveling and GPS data. *Surv Geophys* 37(5):923–936
- Harkins N, Kirby E (2008) Fluvial terrace riser degradation and determination of slip rates on strike-slip faults: an example from the Kunlun fault, China. *Geophys Res Lett* 35:L05406
- Herring TA, King RW, McClusky SC (2015a) GAMIT reference manual, GPS analysis at MIT, Release 10.6. Massachusetts Institute of Technology, Cambridge
- Herring TA, King RW, McClusky SC (2015b) GAMIT reference manual, global Kalman filter VLBI and GPS analysis program, Release 10.6. Massachusetts Institute of Technology, Cambridge
- Hou KM, Lei ZS, Wan FL, Li LM, Xiong Z (2005) Research on the 1879 southern Wudu M8.0 earthquake and its coseismic ruptures. *Earthq Res China* 21(3):295–310 (**in Chinese**)
- Jia W, Liu HC, Liu Y, Yuan DY (2012) Preliminary study on activity of the Wudu-Kangxian fault zone. *Northwest Seismol J* 34(2):142–148 (**in Chinese**)
- Jiang XW, Wang JH, Zhang HH (2003) Coupling between strike-slip faults and basins: the evidence for Cenozoic eastward extrusion of the west Qinling-Songgan block. *Earth Sci Front* 10(3):201–208 (**in Chinese**)
- Kirby E, Harkins N (2013) Distributed deformation around the eastern tip of the Kunlun fault. *Int J Earth Sci* 102:1759–1772
- Kirby E, Harkins N, Wang E, Shi X, Fan C, Burbank D (2007) Slip rate gradients along the eastern Kunlun fault. *Tectonics* 26, TC2010
- Li H, Van der Woerd J, Tapponnier P, Klinger Y, Qi X, Yang J, Zhu Y (2005) Slip rate on the Kunlun fault at Hongshui Gou, and recurrence time of great events comparable to the 14/11/2001,  $M_w = 7.9$  Kokoxili earthquake. *Earth Planet Sci Lett* 237(1–2):285–299
- Li CY, Zhang PZ, Zhang JX, Yuan DY, Wang ZC (2007) Late-Quaternary activity and slip rate of the western Qinling fault zone at Huangxiangou. *Quat Sci* 27(1):54–63 (**in Chinese**)

- Li C, Zhang PZ, Yin JH, Min W (2009) Late Quaternary left-lateral slip rate of the Haiyuan fault, northeastern margin of the Tibetan Plateau. *Tectonics* 28, TC5010
- Li CX, Xu XW, Wen XZ, Zheng RZ, Chen GH, Yang H, An YF, Gao X (2011) Rupture segmentation and slip partitioning of the mid-eastern part of the Kunlun fault, north Tibetan Plateau. *Sci China Earth Sci* 54(11):1730–1745 (**in Chinese**)
- Li YH, Cui DX, Hao M (2015) GPS-constrained inversion of slip rate on major active faults in the northeastern margin of Tibet Plateau. *Earth Sci J China Univ Geosci* 40(10):1767–1780 (**in Chinese**)
- Li YH, Liu M, Wang QL, Cui DX (2018) Present-day crustal deformation and strain transfer in northeastern Tibetan Plateau. *Earth Planet Sci Lett* 487:179–189
- Li HL, Zhang YQ, Dong SW, Zhang JL, Sun YJ, Wang QM (2019) Neotectonics of the Bailongjiang and Hanan faults: new insights into late Cenozoic deformation along the eastern margin of the Tibetan Plateau. *Geol Soc Am Bull.* <https://doi.org/10.1130/B35374.1>
- Liang S, Gan W, Shen C, Xiao G, Liu J, Chen W, Ding X, Zhou D (2013) Three-dimensional velocity field of present-day crustal motion of the Tibetan Plateau derived from GPS measurements. *J Geophys Res Solid Earth* 118(10):5722–5732
- Lin A, Guo J (2008) Nonuniform slip rate and millennial recurrence interval of large earthquakes along the eastern segment of the Kunlun fault, northern Tibet. *Bull Seismol Soc Am* 98(6):2866–2878
- Liu BY (2012) Study on seismologic tectonic and mechanism on Two M8 Historical earthquakes at the southeastern area, Gansu province. Lanzhou Institute of Seismology, China Earthquake Administration, Lanzhou (**in Chinese**)
- Ma SX, Zhang YQ, Li HL, Li JH (2013) The tectonic extrusion of NE Tibet in late Neogene time: evidence from Anhua-Chengxian basin in west Qinling. *Earth Sci Front* 20(4):58–74 (**in Chinese**)
- Mercier JL, Vergely P, Zhang YQ, Hou MJ, Bellier O, Wang YM (2013) Structural records of the Late Cretaceous–Cenozoic extension in Eastern China and the kinematics of the Southern Tan-Lu and Qinling Fault Zone (Anhui and Shaanxi provinces, PR China). *Tectonophysics* 582:50–75
- Peltzer G, Tapponnier P, Zhang ZT, Xu ZQ (1985) Neogene and Quaternary faulting in and along the Qinling Shan. *Nature* 317(10):500–505
- Ren JJ, Xu XW, Yeats RS, Zhang SM (2013) Millennial slip rates of the Tazang fault, the eastern termination of Kunlun fault: implications for strain partitioning in eastern Tibet. *Tectonophysics* 608:1180–1200
- Rui X, Stamps DS (2016) Present-day kinematics of the eastern Tibetan Plateau and Sichuan Basin: implications for lower crustal rheology. *J Geophys Res Solid Earth* 121(5):3846–3866
- Shao YX, Yuan DY, Wang AG, Liang MJ, Liu K, Feng JG (2011) The segmentation of rupture and estimate of earthquake risk along the north margin of western Qinling fault zone. *Seismol Geol* 33(1):79–90 (**in Chinese**)
- Shen ZK, Sun J, Zhang P, Wan Y, Wang M, Bürgmann R, Zeng YH, Gan WJ, Wang QL (2009) Slip maxima at fault junctions and rupturing of barriers during the 2008 Wenchuan earthquake. *Nat Geosci* 2:718–724
- Shen ZK, Wang M, Zeng YH, Wang F (2015) Optimal interpolation of spatially discretized geodetic data. *Bull Seismol Soc Am* 105(4):2117–2127
- Shi W, Dong SW, Hu JM (2020) Neotectonics around the Ordos Block, North China: a review and new insights. *Earth Sci Rev* 200:102969
- Sun HY (2015) Late Quaternary activity of the Qingchuan fault: implications for the tectonic movement mechanism in regional area. Institute of Geology, China Earthquake Administration, Beijing (**in Chinese**)
- Sun JB, Yue H, Shen ZK, Fang LH, Zhan Y, Sun XY (2018) 2017 Jiuzhaigou earthquake: a complicated event occurred in a young fault system. *Geophys Res Lett* 45(5):2230–2240
- Tapponnier P, Peltzer G, Le Dain AY, Armijo R, Cobbold P (1982) Propagating extrusion tectonics in Asia: new insight from simple experiments with plasticine. *Geology* 10:611–616
- Tapponnier P, Xu ZQ, Roger F, Meyer B, Arnaud N, Wittlinger G, Yang JS (2001) Oblique stepwise rise and growth of the Tibet Plateau. *Science* 294:1671
- Van Der Woerd J, Tapponnier P, Ryerson FJ, Meriaux AS, Meyer B, Gaudemer Y, Finkel RC, Caffee MW, Zhao GG, Xu ZQ (2002) Uniform postglacial slip-rate along the central 600 km of the Kunlun Fault (Tibet), from  $^{26}\text{Al}$ ,  $^{10}\text{Be}$ , and  $^{14}\text{C}$  dating of riser offsets, and climatic origin of the regional morphology. *Geophys J Int* 148(3):356–388
- Wang M, Shen ZK (2020) Present-day crustal deformation of continental China derived from GPS and its tectonic implications. *J Geophys Res Solid Earth* 125:e2019JB018774
- Wang EQ, Meng QR, Chen ZL, Chen LZ (2001) Early Mesozoic left-lateral movement along the Longmen Shan fault belt and its tectonic implications. *Earth Sci Front* 8(2):375–384 (**in Chinese**)
- Xu X, Wen X, Chen G, Yu G (2008) Discovery of the Longriba fault zone in eastern Bayan Har block, China and its tectonic implication. *Sci China Ser D Earth Sci* 51(9):1209–1223

- Xu XW, Chen GH, Wang QX, Chen LX, Ren ZK, Xu C, Wei ZY, Lu RQ, Tan XB, Dong SP, Shi F (2017) Discussion on seismogenic structure of Jiuzhaigou earthquake and its implication for current strain state in the southeastern Qinhai-Tibet Plateau. *Chin J Geophys* 60(10):4018–4026 (**in Chinese**)
- Yang XP, Feng XJ, Huang XN, Song FM, Li GY, Chen XC, Zhang L, Huang WL (2015) The late Quaternary activity characteristics of the Lixian-Luojiabu fault: a discussion on the seismogenic mechanism of the Lixian M8 earthquake in 1654. *Chin J Geophys* 58(2):504–519 (**in Chinese**)
- Yu JX, Zheng WJ, Yuan DY, Pang JZ, Liu XW, Liu BY (2012) Late Quaternary active characteristics and slip rate of Pingding-Huama fault, the eastern segment of Guanggaishan-Dieshan fault zone (west Qinling Mountain). *Quat Sci* 32(5):957–967 (**in Chinese**)
- Yuan DY, Zhang PZ, Liu BC, Gan WJ, Mao FY, Wang ZC, Zheng WJ, Guo H (2004) Geometrical imagery and tectonic transformation of late Quaternary active tectonics in northwestern margin of Qinghai-Xizang Plateau. *Acta Geol Sin* 78(2):270–278 (**in Chinese**)
- Yuan DY, Lei ZS, Yang QY, Wang AG, Xie H, Su Q (2014) Seismic disaster features of the 1879 southern Wudu M8 earthquake in Gansu province. *J Lanzhou Univ Nat Sci* 50(5):611–621 (**in Chinese**)
- Zhang YQ, Vergely P, Mercier J (1995) Active faulting in and along the Qinling Range (China) inferred from SPOT imagery analysis and extrusion tectonics of south China. *Tectonophysics* 243:69–95
- Zhang PZ, Wang M, Gan WJ, Deng QD (2003) Slip rates along major active faults from GPS measurements and constraints on contemporary continental tectonics. *Earth Sci Front* 10(Supp.):91–92 (**in Chinese**)
- Zhang GW, Guo AL, Yao AP (2004) Western Qinling-Songpan continental tectonic node in China's continental tectonics. *Earth Sci Front* 11(3):23–32 (**in Chinese**)
- Zhang YG, Zheng WJ, Wang YJ, Zhang DL, Tian YT, Wang M, Zhang ZQ, Zhang PZ (2018) Contemporary deformation of the North China plain from global positioning system data. *Geophys Res Lett* 45:1851–1859
- Zheng WJ, Yuan DY, He WG, Min W, Ren ZK, Liu XW, Wang AG, Xu C, Ge WP, Li F (2013) Geometric pattern and active tectonics in southeastern Gansu province: discussion on seismogenic mechanism of the Minxian-Zhangxian. *Chin J Geophys* 56(12):4058–4071 (**in Chinese**)
- Zheng WJ, Liu XW, Yu JX, Yuan DY, Zhang PZ, Ge WP, Pang JZ, Liu BY (2016) Geometry and late Pleistocene slip rates of the Liangdang-Jiangluo fault in the western Qinling mountains, NW China. *Tectonophysics* 687:1–13
- Zheng G, Wang H, Wright TJ, Lou Y, Zhang R, Zhang W, Wei N (2017) Crustal deformation in the India-Eurasia collision zone from 25 years of GPS measurements. *J Geophys Res Solid Earth* 122:9290–9312
- Zuza AV, Yin A (2016) Continental deformation accommodated by non-rigid passive bookshelf faulting: an example from the Cenozoic tectonic development of northern Tibet. *Tectonophysics* 677–678:227–240

**Publisher's Note** Springer Nature remains neutral with regard to jurisdictional claims in published maps and institutional affiliations.